Using a fiber stretcher as a fast phase modulator in a continuous wave terahertz spectrometer

Axel Roggenbuck,[1,2,*] Komalavalli Thirunavukkuarasu,[1] Holger Schmitz,[1] Jennifer Marx,[1] Anselm Deninger,[2] Ivan Cámara Mayorga,[3] Rolf Güsten,[3] Joachim Hemberger,[1] and Markus Grüninger[1]

[1]*II. Physikalisches Institut, Universität zu Köln, Zülpicher Str. 77, D-50937 Köln, Germany*
[2]*TOPTICA Photonics AG, Lochhamer Schlag 19, D-82166 Gräfelfing, Germany*
[3]*Max-Planck-Institute for Radio Astronomy, Auf dem Hügel 69, D-53121 Bonn, Germany*
**Corresponding author: axel.roggenbuck@toptica.com*

Received December 6, 2011; accepted January 17, 2012;
posted January 24, 2012 (Doc. ID 159508); published March 16, 2012

Continuous wave terahertz spectroscopy based on photomixing offers the attractive feature of detecting both amplitude and phase of the terahertz radiation. Experimentally, it is challenging to achieve sufficient accuracy at a high data acquisition rate. We use two fiber stretchers as fast phase modulators in a symmetric setup. Compared to a mechanical delay stage, the fiber stretchers are rather fast (≈1 kHz), which enables us to record a spectrum up to 1.8 THz with a step size of 1 GHz in only 10 min. We achieve a stability of the optical path difference of around 10 μm and use low-doped Si as an example to demonstrate the performance of our spectrometer.

OCIS codes: 300.6495, 120.6200, 060.5060.

1. INTRODUCTION

Continuous wave terahertz spectroscopy based on photomixing can cover a broad frequency range with high spectral resolution (see, e.g., [1,2]). This technique is based on the superposition of two near-IR lasers, giving rise to an intensity beat in the terahertz range. This optical beat illuminates a first photomixer (the transmitter or source), which emits light at the difference frequency of the two lasers. A second photomixer (the receiver or detector) is used for coherent detection of the terahertz radiation. The detected signal is a photocurrent I_{ph}, which depends both on the amplitude E_{THz} of the terahertz electric field and on the phase difference $\Delta\varphi$ between the incoming terahertz wave and the optical beat signal at the receiver:

$$I_{\mathrm{ph}} \propto E_{\mathrm{THz}} \cos(\Delta\varphi) = E_{\mathrm{THz}} \cos(2\pi\Delta L\nu/c), \qquad (1)$$

where ν denotes the terahertz frequency, c denotes the speed of light, and $\Delta L = L_{\mathrm{Rx}} - (L_{\mathrm{Tx}} + L_{\mathrm{THz}})$ denotes the optical path difference between the receiver arm and the transmitter arm including the terahertz path. In spectroscopy, one wants to determine amplitude and phase of the radiation in a certain frequency range, both for a given sample and for an appropriate reference. This can be achieved by measuring the photocurrent I_{ph} as a function of the phase difference $\Delta\varphi$.

Different solutions have been proposed for the modulation of $\Delta\varphi$. The optical path difference ΔL can be modulated by a conventional mechanical delay stage, e.g., $\Delta L(t) = \Delta L(s=0) + s(t)$ with $s(t) = s_0 \sin(2\pi f_s t)$, where f_s denotes the modulation frequency. This is rather slow because the travel of the delay line, $2s_0$, has to be comparable to or larger than the terahertz wavelength, i.e., 3 mm at 100 GHz. Moreover, a conventional delay stage in the path of the optical beat (L_{Tx} or L_{Rx}) requires a free optical beam [3–8] and thus prevents a compact all-fiber based setup. The alternative position of the delay stage in the terahertz path itself [1]—modulating L_{THz}—is rather problematic because it requires a collimated beam in the terahertz path. Furthermore, modulating the terahertz path strongly affects the standing waves, i.e., parasitic interference effects, which arise from multiple reflections of the terahertz beam [9,10]. Because of these standing waves, also the amplitude E_{THz} depends on the length L_{THz} of the terahertz path, giving rise to significant deviations from a cosine-like behavior of $I_{\mathrm{ph}}(\Delta L)$ if L_{THz} is varied (see Fig. 1).

Alternatively, one may tune $\Delta\varphi$ by shifting the phase of one of the lasers in only one of the two beat paths [11–13]. Compared to the beat signal, the laser wavelength is about three orders of magnitude smaller and thus a delay length of about 1 μm is already sufficient, enabling much faster electro-optical modulation. However, thermal drifts may be of the same order, i.e., 1 μm or even larger, limiting the accuracy and reliability.

In a third approach, $\Delta\varphi$ can be varied for fixed ΔL by scanning the terahertz frequency ν [2,8]. Recently, some of us have shown that this provides an interesting alternative for the determination of the complex dielectric function $\varepsilon(\omega)$ of solid-state samples in a broad frequency range [2]. The drawback of this approach is the measurement speed. It is necessary to measure the oscillating photocurrent with a high density of frequency points, i.e., a step size of about $\Delta\nu = 50$ MHz. In [2], a scanning rate of 2–5 Hz has been used, thus a full scan up to 1.8 THz takes about 2–5 h. For many applications, a much shorter measurement time is desirable or even necessary.

Here, we propose a fast way to modulate ΔL and thus also $\Delta\varphi$ by using fiber stretchers in the path of the optical beat. In contrast to the first approach, the fiber stretchers allow us to

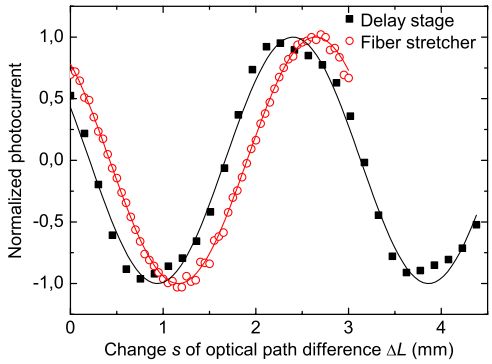

Fig. 1. (Color online) Detected photocurrent at 100 GHz while the optical path difference $\Delta L = \Delta L(s = 0) + s(t)$ is step-scanned with either a fiber stretcher in the path of the optical beat (red, open circles) or a mechanical delay stage in the terahertz path (black squares). The lines represent cosine fits. The phase shift between the two data sets is caused by the difference of $\Delta L(s = 0)$ in the two setups. The small deviations from a cosine shape in the delay-stage data are due to standing waves in the terahertz path.

keep the terahertz path unaffected by the modulation of ΔL while the setup still is all-fiber based. Again, data are acquired with a scanning rate of about 3 Hz, but now a spectrum can be measured with an arbitrary step size $\Delta\nu$. For $\Delta\nu = 1$ GHz, a full spectrum up to 1.8 THz takes only about 10 min. Note that $\Delta\nu$ here plays the role of an effective resolution, whereas the true spectral resolution $\delta\nu$ is of the order of MHz, depending only on the precision and stability of the laser frequencies. This method thus combines all of the essential advantages: the trade-off between measurement speed and effective spectral resolution can be optimized for the specific requirements on a broad scale, it is accurate and reliable, it provides a high frequency selectivity, and it is still compact.

2. EXPERIMENTAL SETUP

The experimental setup is shown in Fig. 2. The laser system and the photomixers are described in [2,14]. Here, we use a combination of two laser diodes with equal center wavelengths of about 780 nm, offering a maximum beat frequency of 1.2 THz. Frequencies of up to 1.8 THz can be reached by using diodes with slightly different center wavelengths [2]. Here, we have chosen a face-to-face configuration of the photomixers, which enables us to achieve small values of L_{THz}, ΔL, and $L_{\mathrm{Rx}} - L_{\mathrm{Tx}}$ simultaneously. This is essential for the phase stability (see below). A face-to-face configuration still yields a reasonable signal because the photomixers' hyperhemispherical Si lenses emit terahertz radiation with a full opening angle of only 10° at 100 GHz, 4° at 350 GHz, and ≤2° between 600 GHz and 1.2 THz (referring to an intensity drop to $1/e$ of the maximum value) [15].

The advanced setup contains two fiber stretchers in the optical path before the photomixers, i.e., where both laser frequencies are superimposed. The two stretchers operate with opposite signs, thus changing the optical path difference ΔL. Each fiber stretcher (Optiphase PZ2-PM3-APC-E-850P) consists of 60 m of polarization-maintaining single-mode fiber wound around a piezo actuator. A voltage applied to the piezo translates linearly into a length change of the fiber and thus changes ΔL. The piezo can be driven with bipolar voltages of up to ±400 V. We typically apply a sinusoidal voltage $U = U_0 \sin(2\pi f_s t)$. Because of the capacitance of the stretchers (100 nF each), the maximum modulation frequency f_s is limited by the maximum output current of the voltage amplifier (200 mA in our case). Additionally, care has to be taken to avoid the mechanical resonance around 18 kHz.

The symmetric setup, which includes one stretcher in the transmitter branch and a second one operated with inverted voltage in the receiver branch, has significant advantages. Compared to a single stretcher, it enables us to double either the length change s of $\Delta L = \Delta L(s = 0) + s$ or the modulation frequency f_s. Moreover, the symmetric setup was chosen to minimize thermal drifts of ΔL and to keep ΔL small ($\ll$1 m) even for a total fiber length of about 120 m. We measured the length change of the optical path difference (for the combination of both stretchers) by analyzing the terahertz signal. From the phase change per fiber-stretcher voltage (see Figs. 3 and 4), we derive $s = U \cdot 17.7\ \mu$m/V. With a voltage amplitude $U_0 = 400$ V, the optical path difference ΔL can be varied by up to $2s_0 = 2U_0 \cdot 17.7\ \mu\mathrm{m/V} \approx 14$ mm. A value of $2s_0 = 3$ mm—corresponding to the wavelength λ at $\nu = 100$ GHz—is obtained for $U_0 = 85$ V.

3. DATA PROCESSING AND ANALYSIS

For generation and detection of terahertz radiation via photomixing, a bias voltage is applied to the transmitter while the photocurrent is measured at the receiver. In order to enhance the sensitivity, one can modulate the bias voltage at the transmitter quickly and apply lock-in detection (in our setup at, e.g., 7.6 kHz [2]). In this case, the fiber stretcher has to be modulated slowly compared to the lock-in frequency or used in step-scan mode, similar to a mechanical delay stage

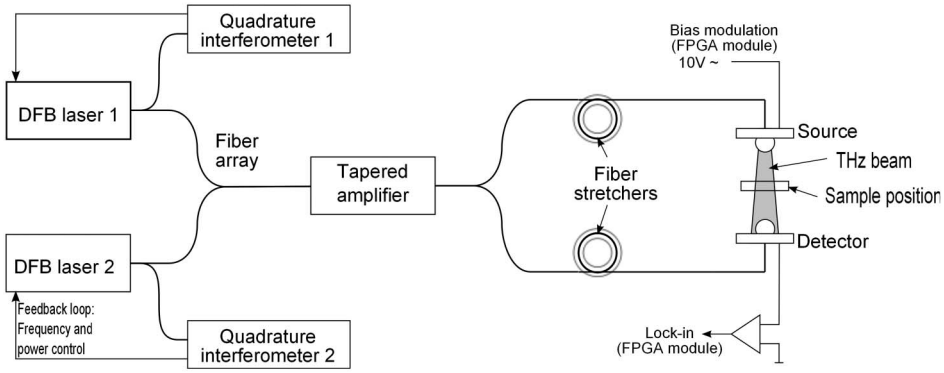

Fig. 2. Setup of the terahertz spectrometer for a face-to-face configuration of the two photomixers.

(see Fig. 1). Alternatively, one may choose a fast modulation of the fiber stretcher in combination with a slower switching of the bias voltage. In the latter scenario, we typically employ a modulation frequency of $f_s = 800$ Hz for the stretcher, and the bias voltage of the transmitter photomixer is inverted at a rate of $2f_{\mathrm{Tx}} = f_s/m$ with $m \in \mathbb{N}$, e.g., $m = 5$ and $f_{\mathrm{Tx}} = 80$ Hz. The modulation of the transmitter bias voltage is necessary to eliminate disturbances correlated with the modulation of the fiber stretcher, e.g., a small variation of the optical power depending on the length of the fiber. In combination with a small voltage offset at the receiver, this disturbance leads to variations of the receiver photocurrent, which can be larger than those due to the terahertz wave. Switching the transmitter voltage inverts the terahertz signal, but not the disturbance.

At the fiber stretchers, a voltage amplitude of $U_0 = 85$ V corresponds to a maximum change $2s_0 = 3$ mm of the optical path difference ΔL. At 1 THz, this already leads to a phase shift of $2s_0/\lambda \cdot 2\pi \approx 10 \cdot 2\pi$, i.e., an effective phase-modulation frequency of $f_{s,\mathrm{eff}} = 2s_0/\lambda \cdot f_s \approx 10 \cdot f_s = 8$ kHz. A high modulation frequency is advantageous since the photocurrent noise density typically decreases with frequency.

The receiver photocurrent is analyzed by so-called signal averaging with a gate width of one stretcher cycle. Typically, we measure about 240 cycles at each THz frequency step, resulting in a net data acquisition rate of about 3 Hz for $f_s = 800$ Hz. The main advantage of signal averaging compared to a standard lock-in technique is that signal averaging does not require the receiver photocurrent to be periodic with a known reference frequency, thus the modulation $s(t)$ of the optical path difference ΔL does not have to be linear in t and the maximum change $2s_0$ of ΔL does not have to be an integer multiple of the terahertz wavelength. Note that this type of signal averaging could also be applied to other fast phase-modulation techniques such as electro-optical phase modulation. Figures 3 and 4 show an example of the averaged signal at $\nu = 600$ GHz. In Fig. 3, we plot the voltage U at the fiber stretcher and the terahertz photocurrent I_{ph} both as a function of time. Around the extrema of U, the optical path difference ΔL and thus also I_{ph} change more slowly. The expected behavior $I_{\mathrm{ph}} = A\cos(2\pi\frac{\nu}{c}\cdot s + \varphi_0)$ is obtained very accurately if we plot I_{ph} versus $s \propto U$ as shown in Fig. 4. The amplitude A and phase φ_0 are derived via a fit (red line in Fig. 4). We emphasize that our fiber stretcher setup—in contrast to a delay stage in the terahertz path—also yields a cosine behavior at low frequencies (see Fig. 1) because standing waves are a serious issue only in the terahertz path, but not in the fiber.

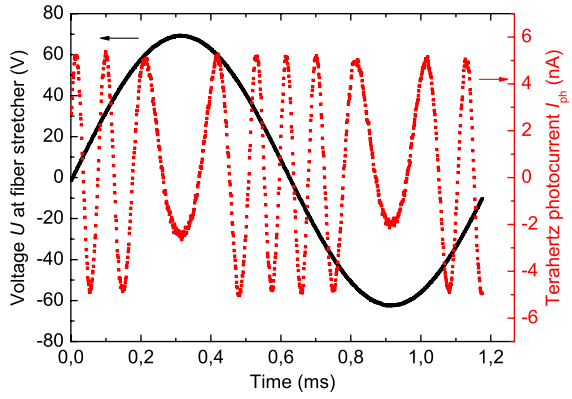

Fig. 3. (Color online) Voltage U at the fiber stretcher and terahertz photocurrent I_{ph} at the receiver photomixer as a function of time for a terahertz frequency of 600 GHz. Here, the frequency of the voltage modulation is $f_s = 800$ Hz and the photocurrent is averaged over ≈240 periods (corresponding to ≈300 ms).

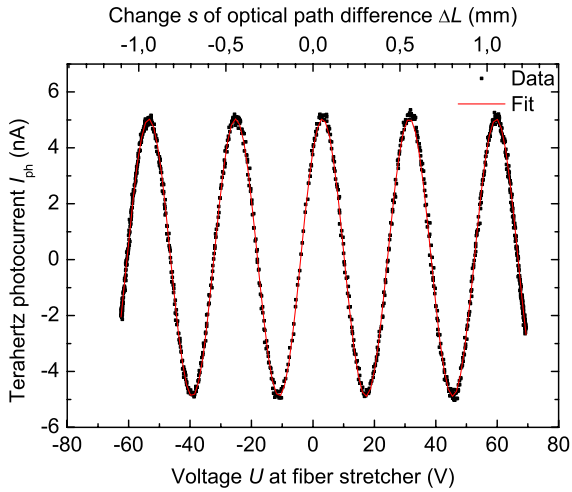

Fig. 4. (Color online) The terahertz photocurrent I_{ph} (same data as in Fig. 3) now plotted as a function of the voltage U at the fiber stretcher, which is proportional to the change s of the optical path difference. A cosine fit with $\lambda = c/\nu \approx 500$ μm describes the data excellently (red line).

The quantities A and φ_0 reflect the terahertz signal and are the final experimentally determined quantities. To derive the optical properties of a sample, such as the complex index of refraction $N = n + \imath k$, one has to compare the quantities A_s and $\varphi_{0,s}$ measured for the sample with those of a reference measurement, A_{ref} and $\varphi_{0,\mathrm{ref}}$, which in a transmission geometry simply corresponds to a measurement on an empty aperture with the sample removed. The transmittance through the sample is $T(\nu) = (A_s(\nu)/A_{\mathrm{ref}}(\nu))^2$, and the phase shift introduced by the sample is $\varphi(\nu) = \varphi_{0,\mathrm{s}}(\nu) - \varphi_{0,\mathrm{ref}}(\nu) + m(\nu)\cdot 2\pi$ with integer $m(\nu)$. The ambiguity in m can be resolved in a broadband measurement. If we, for instance, neglect multiple reflections within the sample of thickness d, one finds $\varphi(\nu) \approx 2\pi(n-1)d\cdot\nu/c$, i.e., φ extrapolates to zero for $\nu \to 0$ and is expected to increase linearly with ν in a frequency range with constant refractive index n. Finally, knowing T and φ as well as the sample thickness d, one can calculate the complex index of refraction, see, e.g., [10].

4. RESULTS

A. Performance of the Spectrometer

The performance of the spectrometer can be evaluated in terms of the stability and dynamic range of the terahertz amplitude, the stability of the phase, the spectral resolution and bandwidth, and the measurement speed. Here, the fiber stretcher setup is compared to the setup without any delay stage (phase modulation by frequency scan), the setup with a delay stage in the terahertz path, and also a setup with a conventional delay stage in the optical path. However, we have never implemented the latter in our setup.

1. Measurement Speed

The central advantage of using a fiber stretcher is the enhanced measurement speed combined with an all-fiber setup. A modulation of the optical path difference of $2s_0 = 3$ mm is obtained for a modulation frequency of ≈1 kHz, whereas a

mechanical delay stage with the same amplitude typically operates at a few hertz or below. We employ a data acquisition rate of a few Hertz, but this already includes an average over about 240 cycles per frequency point. If the phase is modulated by scanning the frequency, a very similar data acquisition rate can be employed but 10 or more frequency points need to be measured to observe a phase shift of at least 2π, which yields one actual data point [2]. The fiber stretcher thus improves the measurement speed by at least an order of magnitude if the same integration times are used. In principle, there are different ways to further reduce the measurement time: one may increase the frequency step size and the fiber stretchers may be operated at rates up to a few kilohertz.

2. Dynamic Range

The dynamic range is the ratio of the maximum signal to the minimum detectable signal. The amplitude of the signal depends on the optics, absorbing windows or apertures within the terahertz beam, the optical power illuminating the photomixers, the bias voltage, and so on. However, for equal conditions, the maximum terahertz amplitude is the same for the system with and without the fiber stretchers and its stability is not significantly influenced by the fiber stretchers. Optical losses in the 60 m long fibers or in the additional fiber connectors are compensated by the laser amplifier (see Fig. 2), thus the stretchers effectively have no influence on the optical power at the photomixers.

The power of the terahertz radiation is about 1 μW at 100 GHz and 50 nW at 1 THz. The corresponding photocurrent amplitude amounts to roughly 100 nA at 100 GHz and a few nanoamperes at 1 THz. For a fiber stretcher modulation at $f_s = 800$ Hz, the minimum detectable terahertz amplitude, i.e., the (receiver) noise floor, has been measured to be of the order of 10 pA. Roughly the same has been found in a setup without fiber stretchers, using lock-in detection with a bias-voltage modulation at a few kHz [2]. Consequently, the dynamic range is also roughly the same for both methods, namely about 85–90 dB at 100 GHz and 55–60 dB at 1 THz [2].

3. Phase Stability

Any uncertainty of the phase translates directly into an uncertainty of the refractive index n, see, e.g., our data on Si below. Therefore, the phase stability is an essential parameter and is discussed in more detail here. According to Eq. (1), an uncertainty of the phase difference $\Delta\varphi = 2\pi\Delta L\nu/c$ can be caused by drifts of either ν or $\Delta L = L_{\mathrm{Rx}} - (L_{\mathrm{Tx}} + L_{\mathrm{THz}})$. The two contributions can be distinguished easily in broadband spectroscopy. In contrast to a drift of ν, a drift of ΔL gives rise to an error of $\Delta\varphi$, which increases linearly in ν. Here, we have used nearly balanced paths, $\Delta L \le 5$ cm, which minimizes the effect of an uncertainty of ν. A drift of ΔL may be caused by either a variation of the laboratory temperature or by a drift of the temperature difference δT between different pieces of the setup. Additionally, one has to consider the uncertainty of the cosine fit of the stretcher data (see Fig. 4).

The fiber stretchers contribute to the uncertainty of ΔL. For the fibers, the drift of the optical path length is dominated by the temperature dependence of the refractive index because the thermo-optic coefficient $\frac{\partial n(\mathrm{SiO_2})}{\partial T} \approx 10^{-5}/\mathrm{K}$ is much larger than the thermal expansion $\alpha(\mathrm{SiO_2}) \approx 0.5 \cdot 10^{-6}/\mathrm{K}$ [16,17]. With a length of 60 m, a single stretcher changes the optical path length by 600 μm/K. It is a significant advantage of the symmetric setup that this has no net effect on ΔL. With one fiber stretcher in the transmitter arm and one in the receiver arm, a common drift of the temperature is irrelevant because it changes the optical path in both arms identically, thus the uncertainty of ΔL is not affected by the fiber stretchers in this case. However, ΔL is still sensitive to a temperature change because of the different lengths or materials of the transmitter and receiver arm. If the photomixers are mounted on, e.g., an Al plate, L_{THz} depends on the thermal expansion coefficient $\alpha_{\mathrm{Al}} \approx 2 \cdot 10^{-5}/\mathrm{K}$. With $L_{\mathrm{THz}} \approx 15$ cm and $L_{\mathrm{Rx}} - L_{\mathrm{Tx}} \approx 10$ cm, we expect and have measured a change of ΔL of a few μm/K. However, this is independent of the fiber stretchers.

For larger values of $L_{\mathrm{Rx}} - L_{\mathrm{Tx}}$ we have observed larger drifts. Therefore, it is advantageous to minimize $L_{\mathrm{Rx}} - L_{\mathrm{Tx}}$, i.e., to use fibers of equal length in the two arms. At the same time, it is advantageous to keep $|\Delta L|$ small in order to minimize the effect of a possible frequency drift. Both can be achieved if L_{THz} is chosen to be small as well.

A change of the temperature difference δT between the two fiber stretchers gives rise to an error of $60\ \mathrm{m} \cdot \frac{\partial n(\mathrm{SiO_2})}{\partial T} \approx 0.6\ \mu\mathrm{m/mK}$. Therefore, we have mounted the two stretchers next to each other with good thermal contact. Additionally, the length of the fibers running to the transmitter and the receiver outside the stretchers has to be taken into account (about 4 m in our setup). This is more than an order of magnitude less than for the stretchers, but it is more difficult to suppress tiny temperature differences in this case because the transmitter and the receiver are spatially separated.

In addition to the drift of ΔL, one also expects a finite drift of the frequency ν because of a finite temperature dependence of the frequency stabilization of the lasers (TOPTICA iScan) of about 10 MHz/K and short-term fluctuations of a few megahertz [1,18]. The resulting change of $\Delta\varphi$ depends on the optical path difference ΔL. For a balanced setup with $\Delta L = 0$, the phase becomes insensitive to drifts of ν. For $\Delta L = 5$ cm, a frequency drift of 10 MHz leads to a phase drift of ≈0.01, which in turn is equivalent to a drift of ΔL of 5 μm at 100 GHz, or 1 μm at 500 GHz. Therefore, a high frequency resolution on the order of 10 MHz is necessary for a precise determination of the terahertz phase, in particular at low terahertz frequencies. The frequency resolution is not influenced by the fiber stretchers, but we emphasize that the fiber stretchers (as the use of any delay line) principally allow us to balance the spectrometer and thereby minimize the effect of frequency drifts on the phase.

We have measured $\Delta\varphi$ as a function of time t over 1 h by cycling the frequency in steps of 50 GHz under standard laboratory conditions without active stabilization of the ambient temperature. Assuming that the drift of ν is negligible, we can calculate the corresponding drift of $\Delta L = \Delta\varphi/2\pi \cdot c/\nu$, see Fig. 5. The data clearly show the same long-term drift of ΔL for all frequencies. Thus, the uncertainty of $\Delta\varphi$ is indeed dominated by the uncertainty of ΔL, not of ν, as expected for $\Delta L \le 5$ cm. The magnitude of the long-term drift (1 h) amounts to about 10 μm. According to the discussion above, this long-term drift can be attributed to both a drift of the common temperature as well as to a drift of the temperature difference between different parts of the setup. The data show

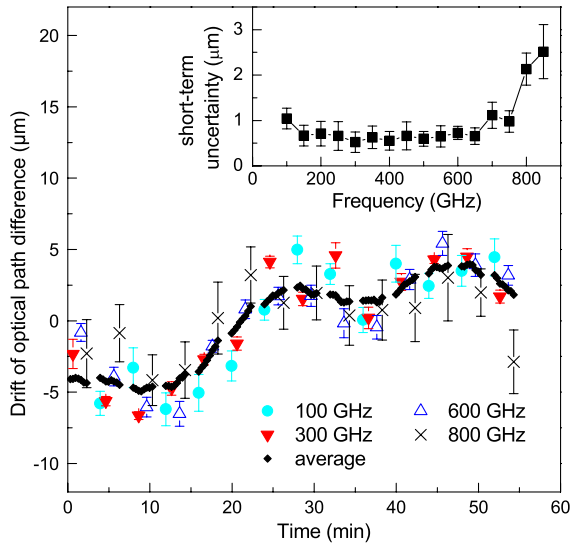

Fig. 5. (Color online) Drift of the optical path difference ΔL versus time. The data points and error bars represent the mean value and standard deviation of about 20 consecutive values of ΔL measured within about 10 s at constant frequency. Small diamonds show the drift of ΔL averaged over all frequencies. Inset: Short-term (10 s) uncertainty of the optical path difference ΔL versus frequency ν, calculated for each frequency from about 15 values (error bars in the main panel). Error bars in the inset represent the standard deviation.

that the temperature difference between the two fiber stretchers is stable within 20 mK.

The uncertainty of ΔL on the time scale of a few seconds is given by the error bars in the main panel of Fig. 5. The frequency dependence of these short-term fluctuations is plotted in the inset of Fig. 5. We observe an uncertainty of about 1 μm between 100 and 650 GHz. The increase above 650 GHz can be attributed to the uncertainty of the fit of the stretcher data due to photocurrent noise (see Fig. 4). This uncertainty increases with decreasing terahertz signal. The increase at the low-frequency side is due to the uncertainty of the frequency ν.

Summarizing the discussion of phase stability, our setup is capable of measuring the optical path difference induced by a sample with an uncertainty of about 10 μm. The corresponding uncertainty of the refractive index n depends on the sample thickness (see below). The essential points for an accurate determination of the phase are the balanced length difference of $\Delta L \ll 1$ m, the symmetric setup using two fiber stretchers, and the short measurement time of about 10 minutes for a full spectrum.

4. *Spectral Resolution and Bandwidth*

The spectral resolution and bandwidth are determined by the characteristics of the employed lasers, both for a system using a fiber stretcher or a conventional mechanical delay stage. However, if $\Delta\varphi$ is modulated by varying ν for fixed ΔL, the effective resolution is given by the period of the interference fringes, i.e., typically an order of magnitude worse. This is clearly seen in Fig. 6 where the frequency dependence of the photocurrent I_{ph} is plotted around 100 and 600 GHz, once determined using the fiber stretcher and once measured for a fixed optical path difference ΔL. The fiber-stretcher measurement yields the amplitude of I_{ph} for each frequency ν and thus traces the envelope of the interference fringes that we obtain in a measurement with $\Delta L = \mathrm{const}$. These data clearly show the difficulties encountered if the dielectric properties of a sample are determined in a setup with $\Delta L = \mathrm{const}$, at least at low frequencies. The fringes are shifted in the data of sample and reference, and therefore the envelope has to be interpolated to reveal the sample properties [2]. At low frequencies, the envelope is rather irregular due to the enhanced role of standing waves, thus an interpolation introduces significant errors. In contrast, standing waves which are not caused or influenced by the sample cancel out if sample and reference are compared at the same frequency, as done in the measurement with the fiber stretcher. Note that complete cancellation requires the time between sample and reference measurement to be short enough to eliminate drifts.

B. Representative Data on Si

We demonstrate the performance of our spectrometer using the well-studied example of low-doped Si. In order to suppress standing waves at low frequencies, the data below 700 GHz was measured with absorbers in the terahertz path between transmitter and sample as well as between receiver and

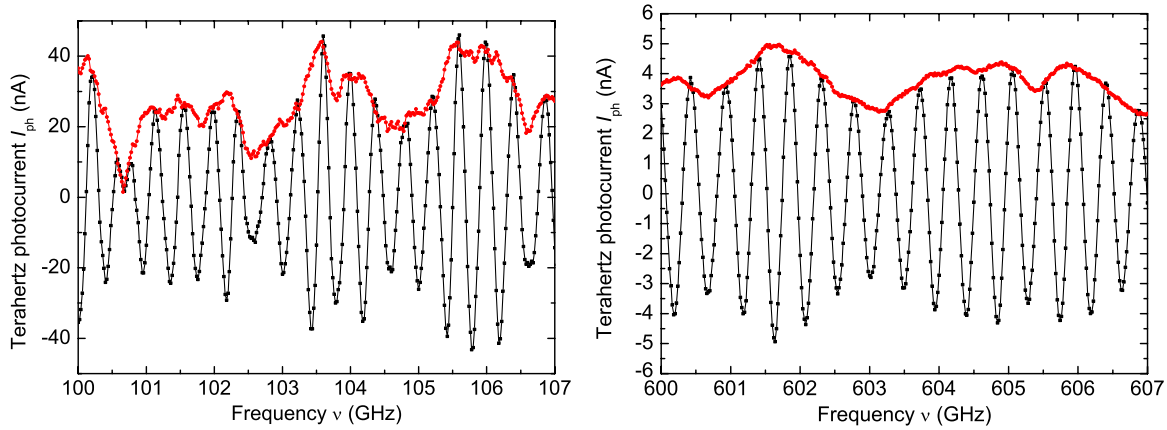

Fig. 6. (Color online) Terahertz photocurrent I_{ph} at about 100 GHz (left) and 600 GHz (right) measured either using the fiber stretchers (red) or the frequency-scanning method with constant ΔL (black). In the latter case, the period of the interference fringes depends on ΔL. A reasonable effective frequency resolution requires a small period and thus a rather large ΔL (about 0.6 m for this data set), which again is unfavorable for a high phase accuracy. The modulation of the envelope with about 2 GHz can be attributed to multiple reflections between the photomixers, which here have been used in a face-to-face setup with a distance of about 8 cm.

sample. We measured the transmittance $T(\nu)$ and the phase shift $\varphi(\nu)$ induced by the sample (see above) at room temperature with a frequency step size of 1 GHz. The data were averaged over 15 runs. In Fig. 7, we plot $T(\nu)$ and the effective optical path length $L_{\text{eff}} = \Delta L_s - \Delta L_{\text{ref}} = (\varphi/2\pi) \cdot c/\nu$. Both data sets show strong Fabry–Perot fringes due to multiple reflections within the highly transparent sample.

The fact that L_{eff} is nearly constant (besides the Fabry–Perot fringes) indicates that the refractive index n varies only weakly with frequency within the measured frequency range. If the sample thickness d is known, e.g., from a mechanical measurement, one can obtain a first estimate of n from either $T(\nu)$ or L_{eff}. At the maxima of the interference fringes observed in $T(\nu)$, $2n \cdot d$ equals an integer multiple of the wavelength. We find $n \cdot d = (1.710 \pm 0.004)$ mm and with the mechanically measured thickness of $d = (505 \pm 3)$ μm we calculate $n = 3.39 \pm 0.03$, in agreement with [19,20]. Here, the uncertainty of n is dominated by the uncertainty of d, and the dispersion of n in the measured frequency range is smaller than the error of n. Independently, we may use $L_{\text{eff}} \approx (n-1) \cdot d$ and $L_{\text{eff}} = (1.21 \pm 0.02)$ mm from Fig. 7 to find $n = 3.40 \pm 0.05$, in excellent agreement with the result derived from $T(\nu)$. The larger error reflects the uncertainty of L_{eff}.

In the following, we discuss the frequency dependence of the optical constants. We have fitted $T(\nu)$ and $L_{\text{eff}}(\nu)$ simultaneously using a Drude–Lorentz model. Note that this analysis does not require any knowledge about the sample thickness. In the model, we assume a small Drude contribution of free carriers and a constant dielectric function at high frequencies. The free carriers suppress the amplitude of the interference fringes in $T(\nu)$ at low frequencies. The good agreement of the fit (red lines in Fig. 7) with both data sets demonstrates the Kramers–Kronig consistency of our data. The fit yields a plasma frequency of $\nu_p \approx 292$ GHz, a damping constant of $\gamma/2\pi \approx 1.08$ THz, and a sample thickness of $d = 506$ μm. The latter agrees very well with the mechanically measured value of $d = (505 \pm 3)$ μm. The fit result for the frequency dependence of the optical constants $n(\nu)$ and $k(\nu)$ is displayed in the inset of Fig. 7. With an effective hole mass of $m^* = 0.37 m_0$ [19], where m_0 is the free electron mass, and the free-space permittivity ε_0, we find a carrier density of $N/V = \varepsilon_0 \cdot m^* \cdot (2\pi\nu_p/e)^2 \approx 3.9 \cdot 10^{14}/\text{cm}^3$, a DC conductivity of $\sigma_{\text{D.C.}} = \varepsilon_0 \cdot (2\pi\nu_p)^2/\gamma \approx 0.044/(\Omega\ \text{cm})$, and a mobility of $\mu = e/\gamma m^* \approx 0.70 \cdot 10^3\ \text{cm}^2/(\text{Vs})$, in agreement with [19]. The optically determined value of the DC conductivity is in excellent agreement with the directly measured resistivity at room temperature of $1/\rho = 0.047/(\Omega\ \text{cm})$.

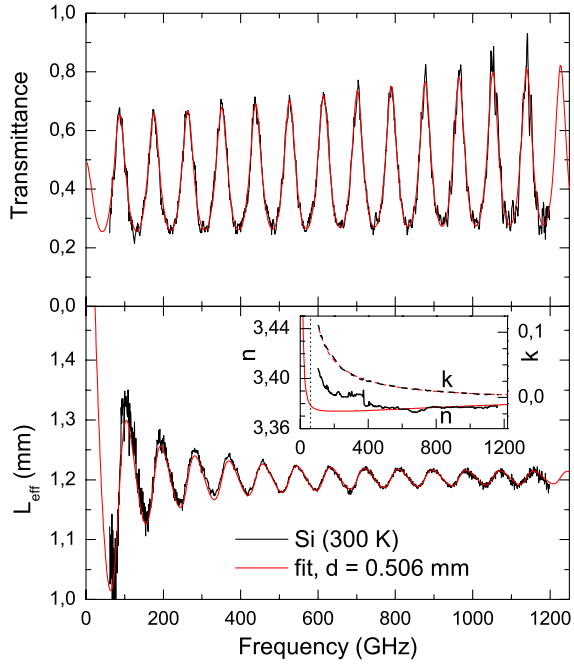

Fig. 7. (Color online) Transmittance (top panel) of a single crystal of Si and effective optical path length introduced by the sample (bottom panel) at 300 K. Inset: refractive index n (left axis, solid lines) and extinction coefficient k (right axis, dashed lines) as derived from a Drude model (red) and from a fit of small frequency ranges (black).

Finally, we address the accuracy of our result for the optical constants. Above we assumed a Drude model with a single oscillator at zero frequency, fitting the entire frequency range at once. For comparison, we studied the optical constants for each frequency ν_0. More precisely, we analyzed a small frequency range of $\nu_0 \pm 50$ GHz in order to utilize the information contained in the Fabry–Perot fringes. In each range, we obtained $n(\nu_0)$ and $k(\nu_0)$ by fitting the data with a Drude–Lorentz model with three oscillators. As long as all relevant features in the data have a width larger than the fitted range of 100 GHz, this approach in principle is capable of describing deviations from a Drude line shape reliably. However, we find excellent agreement with the result from the Drude model discussed above (see inset of Fig. 7). Within the measured frequency range, n varies by only about 1%, whereas k is changing by more than an order of magnitude. Based on the Kramers–Kronig relations, the strong increase of k with decreasing frequency implies that also n increases at low frequencies, but this occurs mainly below 60 GHz, the lower frequency limit of our data.

5. CONCLUSION

In a continuous wave terahertz spectrometer based on photomixing, fast modulation of the phase has been achieved by the implementation of two fiber stretchers. The maximum change of the optical path length amounts to 14 mm. The main advantage is the enhanced measurement speed. With a net data acquisition rate of about 3 Hz, a full spectrum up to 1.8 THz with a frequency step size $\Delta\nu = 1$ GHz is measured in only 10 min. This is essential for many applications, e.g., temperature- or magnetic-field-dependent measurements. Moreover, a short measurement time reduces the effect of thermal drifts of the setup. Even though each fiber stretcher has a total fiber length of 60 m, the optical path difference is stable within around 10 μm due to the use of a symmetric setup with $\Delta L \ll 1$ m and because of the short measurement time. Together with the high frequency stability of around 10 MHz of our spectrometer, this offers a precise determination of the terahertz phase. This, in turn, allows for highly accurate measurements of a sample's complex refractive index and thickness, as demonstrated here for low-doped Si.

ACKNOWLEDGMENTS

We express our gratitude to T. Göbel (TU Darmstadt, now HHI Berlin) for experimental support and stimulating discussions. This project is supported by the Deutsche Forschungsgemeinschaft via Sonderforschungsbereich 608.

REFERENCES

1. A. J. Deninger, T. Göbel, D. Schönherr, T. Kinder, A. Roggenbuck, M. Köberle, F. Lison, T. Müller-Wirts, and P. Meissner, "Precisely tunable continuous-wave terahertz source with interferometric frequency control," Rev. Sci. Instrum. **79**, 044702 (2008).
2. A. Roggenbuck, H. Schmitz, A. Deninger, I. Cámara Mayorga, J. Hemberger, R. Güsten, and M. Grüninger, "Coherent broadband continuous-wave terahertz spectroscopy on solid-state samples," New J. Phys. **12**, 043017 (2010).
3. S. Verghese, K. A. McIntosh, S. Calawa, W. F. Dinatale, E. K. Duerr, and K. A. Molvar, "Generation and detection of coherent terahertz waves using two photomixers," Appl. Phys. Lett. **73**, 3824–3826 (1998).
4. A. Nahata, J. T. Yardley, and T. F. Heinz, "Free-space electro-optic detection of continuous-wave terahertz radiation," Appl. Phys. Lett. **75**, 2524–2526 (1999).
5. K. J. Siebert, H. Quast, R. Leonhardt, T. Löffler, M. Thomson, T. Bauer, H. G. Roskos, and S. Czasch, "Continuous-wave all-optoelectronic terahertz imaging," Appl. Phys. Lett. **80**, 3003–3005 (2002).
6. I. S. Gregory, W. R. Tribe, B. E. Cole, C. Baker, M. J. Evans, I. V. Bradley, E. H. Linfield, A. G. Davies, and M. Missous, "Phase sensitive continuous-wave THz imaging using diode lasers," Electron. Lett. **40**, 143–145 (2004).
7. R. Mendis, C. Sydlo, J. Sigmund, M. Feiginov, P. Meissner, and H. L. Hartnagel, "Coherent generation and detection of continuous terahertz waves using two photomixers driven by laser diodes," Int. J. Infrared Milli. Waves **26**, 201–207 (2005).
8. G. Mouret, S. Matton, R. Bocquet, D. Bigourd, F. Hindle, A. Cuisset, J. F. Lampin, K. Blary, and D. Lippens, "THz media characterization by means of coherent homodyne detection, results and potential applications," Appl. Phys. B **89**, 395–399 (2007).
9. B. P. Gorshunov, A. A. Volkov, A. S. Prokhorov, I. E. Spektor, J. Akimitsu, M. Dressel, G. Nieuwenhuys, S. Tomic, and S. Uchida, "Terahertz BWO spectroscopy of conductors and superconductors," Quantum Electron. **37**, 916–923 (2007).
10. G. Kozlov and A. Volkov, "Coherent Source Submillimeter Wave Spectroscopy," in *Millimeter and Submillimeter Wave Spectroscopy of Solids*, G. Grüner, ed., Topics in Applied Physics (Springer, 1998), Vol. **74**, pp. 51–110.
11. A. M. Sinyukov, Z. Liu, Y. L. Hor, K. Su, R. B. Barat, D. E. Gary, Z.-H. Michalopoulou, I. Zorych, J. F. Federici, and D. Zimdars, "Rapid-phase modulation of terahertz radiation for high-speed terahertz imaging and spectroscopy," Opt. Lett. **33**, 1593–1595 (2008).
12. T. Göbel, D. Schoenherr, C. Sydlo, M. Feiginov, P. Meissner, and H. L. Hartnagel, "Continuous-wave terahertz system with electro-optical terahertz phase control," Electron. Lett. **44**, 863–864 (2008).
13. T. Göbel, D. Schoenherr, C. Sydlo, M. Feiginov, P. Meissner, and H. L. Hartnagel, "Single-sampling-point coherent detection in continuous-wave photomixing terahertz systems," Electron. Lett. **45**, 65–66 (2009).
14. I. Cámara Mayorga, E. A. Michael, A. Schmitz, P. van der Wal, R. Güsten, K. Maier, and A. Dewald, "Terahertz photomixing in high energy oxygen- and nitrogen-ion-implanted GaAs," Appl. Phys. Lett. **91**, 031107 (2007).
15. The opening angle was measured using the knife-edge method; i.e., a metallic edge was translated through the THz beam perpendicular to the propagation direction. The total power behind the edge was focused onto the detector by using two lenses, and a Gaussian beam profile was assumed for the data analysis.
16. G. Ghosh, "Temperature dispersion of refractive indexes in some silicate fiber glasses," IEEE Photon. Technol. Lett. **6**, 431–433 (1994).
17. S. Chang, C.-C. Hsu, T.-H. Huang, W.-C. Chuang, Y.-S. Tsai, J.-Y. Shieh, and C.-Y. Leung, "Heterodyne interferometric measurement of the thermo-optic coefficient of single mode fiber," Chin. J. Phys. **38**, 437–442 (2000).
18. A. Roggenbuck, A. Deninger, I. Cámara Mayorga, H. Schmitz, J. Hemberger, F. Lison, and M. Grüninger, "CW terahertz spectrometer with high-precision frequency control," in *Conference on Lasers and Electro-Optics/International Quantum Electronics Conference*, OSA Technical Digest (CD) (Optical Society of America, 2009), paper CMX3.
19. T. Jeon and D. Grischkowsky, "Nature of conduction in doped silicon," Phys. Rev. Lett. **78**, 1106–1109 (1997).
20. D. Grischkowsky, S. Keiding, M. Van Exter, and Ch. Fattinger, "Far-infrared time-domain spectroscopy with terahertz beams of dielectrics and semiconductors," J. Opt. Soc. Am. B **7**, 2006–2015 (1990).